Magnetic properties of a nanocrystalline material for current derivative sensors of magnets protection systems

24th IMEKO TC4 International Symposium
22nd International Workshop on ADC and DAC Modelling and Testing
IMEKO TC-4 2020
Palermo, Italy, September 14-16, 2020

Magnetic properties of a nanocrystalline material for current derivative sensors of magnets protection systems

Pasquale Arpaia[1], Marco Buzio[2], Ernesto De Matteis[2], Alessandro Parrella[2], Mariano Pentella[2,3]

[1]*Department of Electrical Engineering and Information Technology, University of Naples Federico II, Naples, Italy*
[2]*Technology Department, CERN, Geneva, Switzerland*
[3]*Department of Applied Science and Technology, Politecnico di Torino, Turin, Italy*

***Abstract* – Nanocrystalline materials are becoming ever more broadly used in transformer-based transducers due to their low losses, high relative permeability and high saturation flux density. In this paper, the magnetic characterization of one of these materials is presented by highlighting its influence on the performance of a current derivative sensor. This sensor was recently prototyped at CERN in the framework of the consolidation activity on the quench protection of superconducting magnets for the high-luminosity upgrade of the Large Hadron Collider. The performance is analyzed in terms of linearity and dynamic response.**

I. INTRODUCTION

Nowadays, due to the ever-higher frequencies employed in a broad range of applications (i.e. power electronics), the quest for materials capable of working in wide frequency ranges and having reduced power losses, high permeability values and high saturation level has become crucial. Materials such as ferrites, Fe-Ni, Fe-Si, permalloys, supermalloys, powder cores made from milled nanocrystalline and amorphous materials belong to this category and are broadly employed, as reported in the vast dedicated literature [1, 2, 3, 4].

For the high-luminosity upgrade of the Large Hadron Collider (LHC) [5], a new generation of superconducting magnets such as the Nb_3Sn-based MQXF inner triplet quadrupole magnets and the MBH-11 T dipoles will be installed in the accelerator [6]. The installation, firstly, requires a series of consolidation activities on the existing systems, including the upgrade of the existing quench protection systems, which are crucial components necessary to protect the superconducting magnets from undesired events of quench. These systems are conceptually made of two parts: the quench detection and the magnet protection system, the latter made of active protection elements triggered and coordinated by the quench detection system (i.e. heater discharge power supplies and energy extraction systems) and passive elements (i.e. extraction resistors, bypass diodes, etc.) [7]. These protection features will be guaranteed by a broad variety of new developed custom-made solutions [8]. As reported in [9], a new method for the quench detection has been presented for the 600 A corrector magnet circuits of the LHC and the protection of the IPQ (Individual Powered Quadrupole) magnets. The proposed technology is a transformer-based transducer, whose layout is shown in Fig. 1, that detects the quench by current derivative measurement instead of the classical techniques based on coil voltage measurements.

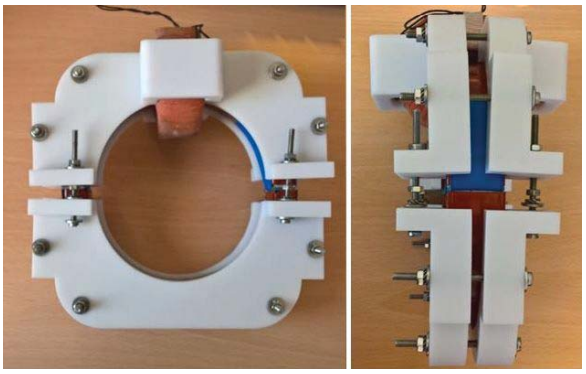

Fig. 1. A photograph of the sensor described in [9].

A nanocrystalline material known under the commercial name Vitroperm500 F® [10] was chosen as magnetic core due to the declared permeability of more than 50000, the high saturation flux density value of about 1.2 T, and low power losses. These parameters are crucial because the sensor will be mainly used for two applications: i) the measurement of the derivative of current carried in the main magnet circuit, with ramp rate values ranging in the order of few A/s and ii) the quench detection feature with values of the derivative over 100 A/s. Hence, good linearity within a range from DC to a few hundreds of Hz is required.

The twofold goal of this paper is i) the assessment of the material magnetic properties and ii) a characterization in terms of linearity and dynamic response carried out by introducing two 3-mm air gaps on a second identical test

specimen to recreate the same sensor operative conditions.

II. MAGNETIC MATERIAL CHARACTERIZATION

The magnetic characterization of the material was performed on a toroidal test specimen by using the flux-metric method, according to the standard IEC 60404-4 [11].
The measurement system layout is shown in Fig. 2

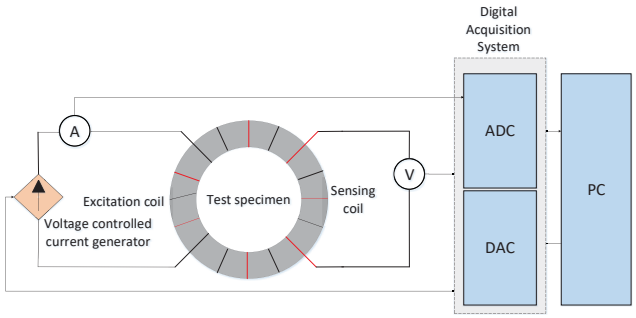

Fig. 2. Measurement system layout

The test specimen is magnetized by an excitation coil made of N_e turns and powered by a voltage-controlled current generator. An N_s-turns sensing coil detects the induced voltage. From the current measurement $i(t)$, the magnetic field is evaluated as:

$$H(t) = \frac{N_e i(t)}{2\pi r_0} \tag{1}$$

where r_0 is the log-mean radius of the toroidal test specimen. From the voltage measurement $v(t)$, the magnetic flux $\Phi(t)$, linked with the N_s sensing turns, is calculated as:

$$\Phi(t) = \int_{t_0}^{t} v(\tau) d\tau \tag{2}$$

This yields to the expression of the magnetic flux density, $B(t)$:

$$B(t) = \frac{1}{A_s}\left(\frac{\Phi(t)}{N_s} - \mu_0 H(t) A_a\right) \tag{3}$$

where A_s is the cross-sectional area of the specimen, $A_a = A_t - A_s$ is the portion of the coil area A_t occupied by the air.
The initial magnetization curve is retrieved by evaluating the point pairs (H_i,B_i) corresponding to the top points of the nested hysteresis loop. The evaluation is carried out by searching the points corresponding to the maximum energy density, evaluated as $H(t)B(t)$.
Starting from the point pairs, the relative permeability is obtained as:

$$\mu_r(H_i) = \frac{B_i}{\mu_0 H_i} \tag{4}$$

where μ_0 is the vacuum permeability.
The results of the DC magnetic characterization are shown in Fig. 3 and Fig. 4.

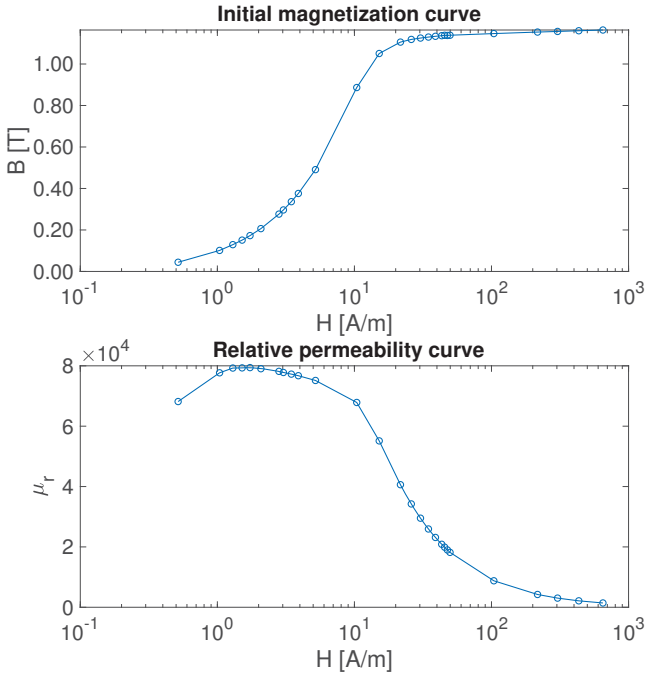

Fig. 3. Top) Initial magnetization curve of Vitroperm500 F® Bottom) Relative permeability curve

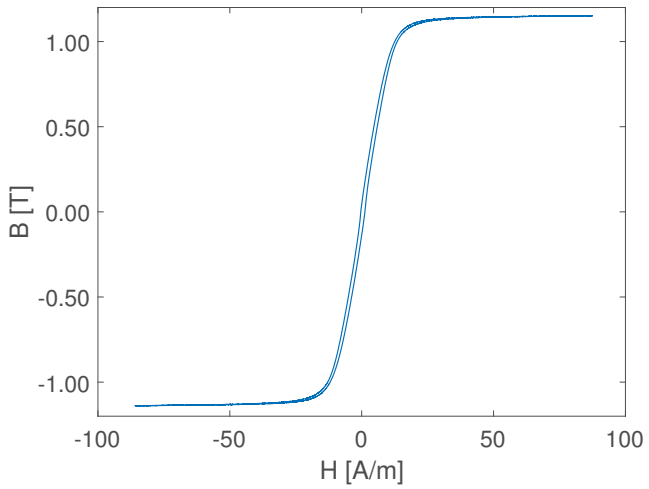

Fig. 4. Hysteresis loop of Vitroperm500 F®

The material presents a saturation flux density equal to 1.151 T, a coercive field of 1.229 A/m, a remanent field of 0.044 T. The specific energy loss per each hysteresis cycle is 3.047 J/m^3. The relative permeability peak is 79,410. The initial permeability was not measured due to the low resolution of the measurements below 0.50 A/m.
In comparison with classical ferromagnetic steels,

Vitroperm500F® presents lower saturation point but higher permeability (one order of magnitude higher) and a lower coercive field value (lower of a factor of 20 in the best case). Although a higher saturation point would allow increasing the operative range of the sensor, non-negligible hysteresis phenomena may occur when using classical ferromagnetic steels as iron core of the sensor. These phenomena can either be a cause of non-linearities or limit the sensor bandwidth.

III. INFLUENCE OF THE AIR-GAP ON THE SENSOR PERFORMANCE

A second toroidal test specimen, with two 3-mm air gaps, was used to recreate the layout of the current derivative sensor and carry out a study on the sensor performance in terms of linearity and sensitivity.

The specimen was installed as a current sensor on a HOLEC power converter [12], capable of delivering currents up to 5500 A. The signal was then measured by a 100-turns sensing coil. A photograph of the setup is shown in Fig. 5.

Fig. 5. Test specimen installed on the power converter cables.

The specimen was tested by adopting the measurement method described in the previous section. The current-to-field transfer function is shown in Fig. 6.

The current-to-field transfer function saturates at 1 T, in correspondence of the material saturation point. The difference lies in the initial branch, where the behavior can be approximated as linear: this was caused by the presence of the two air-gaps. Moreover, the air-gaps made negligible the hysteresis of the material, which has an overall effect below 10^{-5} T.

The linearity of the sensor is shown in Fig. 7, where the values of the voltage are plotted as a function of the current for five different ramp rates.

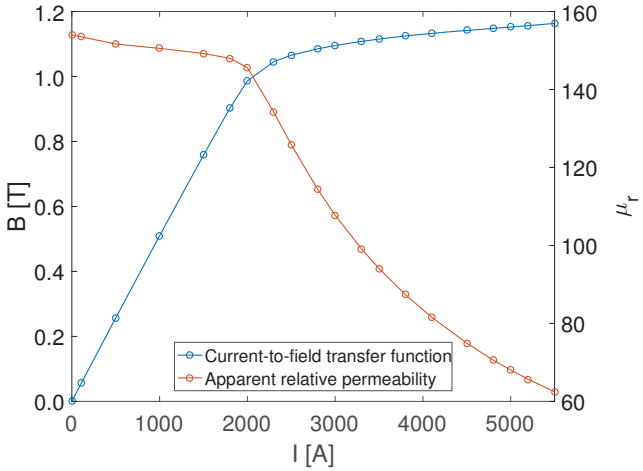

Fig. 6. Sensor current-to-field transfer function and apparent permeability curve.

The curves between 40 and 500 A/s correspond to a real operative situation that the sensor will undergo after the installation on the LHC magnets. The voltage increases linearly with the ramp rate of the current up to 2000 A. The vertical branches, where the voltage drops to zero correspond to the current's plateaux. In the current range [2000 2400] A, the sensor undergoes a transition phase before reaching the full-saturation above 2500. This behavior is also highlighted in Fig. 8.

The blue curve represents the voltage-to-ramp-rate sensor characteristics for current levels lower than 2000 A. The red one, represents the situation for currents above 2500 A. The plots confirm the situation already shown in Fig. 7, where the voltage abruptly decreases in saturation with the slope of the voltage-to-ramp-rate sensor characteristics passing from 0.0146 to 0.00086 mVs/A and thus, decreasing of a factor of about 20.

However, the voltage-to-ramp-rate sensor characteristic is not linear for all the ramp rate levels. In fact, by increasing the current ramp rate, higher- order effects cannot be considered as negligible. For instance, the curve at 5000 A/s, presents some extra lag effects in the very low current region due to the eddy currents circulationg in the core. Nonetheless, at increasing ramp rates, it may not be worth employing this kind of sensor and air coils such as Rogowski's coils [13, 14] may show better performance.

The operative range of the sensor, highly dependent on the saturation current, can be modified by regulating the air-gap length. A higher air-gap length determines a higher saturation current and therefore extends the operative range of the sensor. However, the air-gap length influences as well the sensitivity of the sensor as well. In fact, increasing the air-gap improves the linearity and therefore extends the operative range, but sacrificing the sensitivity. This drawback may be partially mitigated by increasing the number

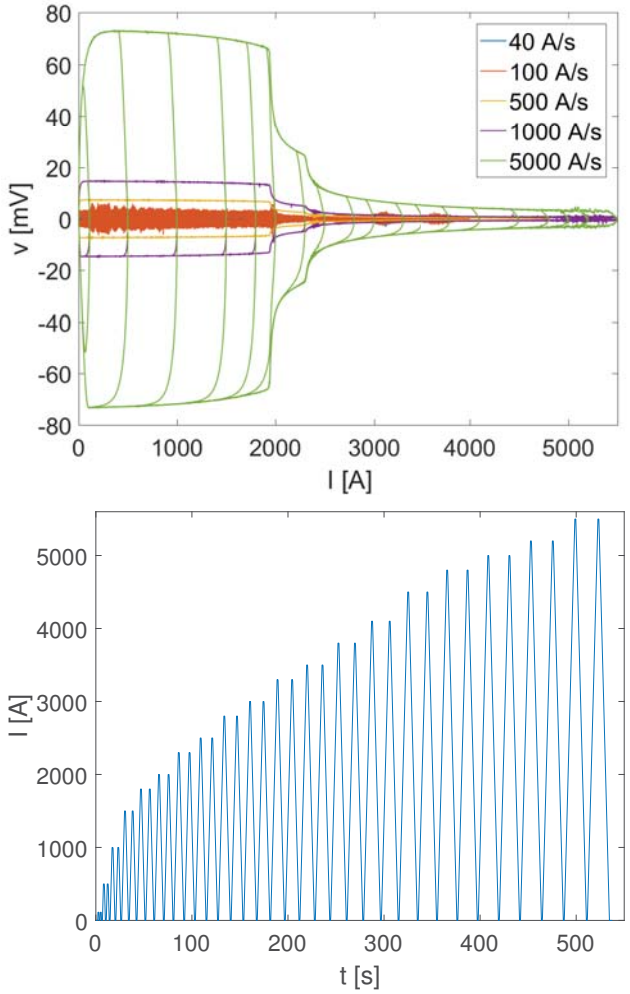

Fig. 7. Top) Voltage-to-current sensor characteristic. Bottom) Current test waveform at a 500 A/s ramp-rate

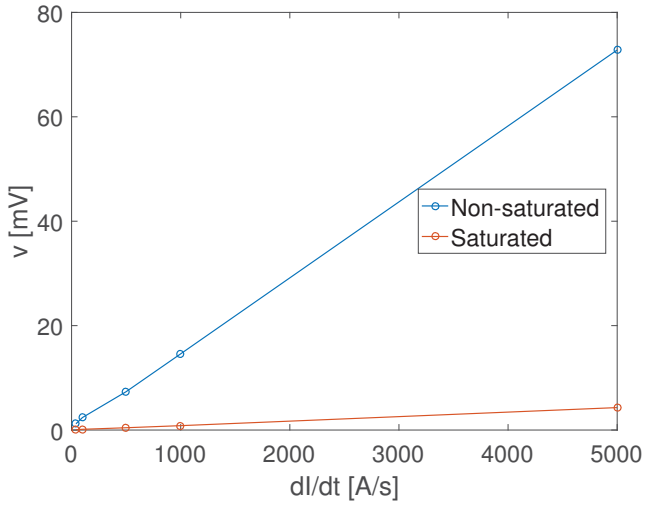

Fig. 8. Voltage-to-ramp-rate sensor characteristic before (blue) after (red) the saturation current.

of sensing turns but at the cost of increasing the measurement noise as well and thus, making the adopted solution iunconvenient. Hence, when designing the sensor, a proper trade-off between linearity and sensitivity needs to be sought.

IV. CONCLUSIONS

In this paper, the magnetic characterization of an innovative nanocrystalline material, Vitroperm500F®, was presented. The material was proposed as iron core for the realization of innovative current derivative sensors to be employed in superconducting magnet protection systems as part of the consolidation activities for the high-luminosity upgrade of the Large Hadron Collider, HL-LHC.

The magnetic characterization of the material was performed on a toroidal test specimen by adopting a standard IEC test procedure. In comparison with a classical ferromagnetic steels, the material exhibits a lower saturation point and a lower coercive field (at least 20 times lower). This improves the sensor performance in terms of linearity and bandwidth.

A similar test specimen realized by introducing two 3-mm air-gaps was tested in order to replicate the sensor layout and characterize it. The results showed a linear behavior up to a current level of 2000 A with negligible hysteresis. At current levels higher than 2500 A, the sensor saturates and the sensitivity abruptly drops of a factor of 20.

The operative range of the sensor can be extended by modifying the air-gap length. Increasing the air-gap determines an higher saturation current. However, as a result, the sensitivity will be inevitably sacrificed.

As future perspectives, the results on the gaped specimen showed that the sensor design is strongly dependent upon the identification of the optimal working point of the core, either in terms of current range or sensitivity. In conclusion,the sensor built with a Vitroperm500F® core is very promising to be used as a quench detector for the IPQ magnets, having a nominal current up to 6000 A.

V. ACKNOWLEDGEMENTS

The authors thank R. Beltron Mercadillo and X. Gontero for the technical support, and J. Vella Wallbank for the help with the gaped specimen measurements.

REFERENCES

[1] D. Grybos, J. Leszczynski, C. Swieboda, M. Kwiecien, R. Rygal, M. Soinski, W. Pluta, Magnetic properties of composite cores made of nanocrystalline material for high frequency inductors and transformers, in: Innovative Materials and Technologies in Electrical Engineering (i-MITEL), 2018, IEEE, 2018, pp. 1–6.

[2] A. Krings, A. Boglietti, A. Cavagnino, S. Sprague, Soft magnetic material status and trends in electric

machines, IEEE transactions on industrial electronics 64 (3) (2017) 2405–2414.

[3] M. E. McHenry, M. A. Willard, D. E. Laughlin, Amorphous and nanocrystalline materials for applications as soft magnets, Progress in materials Science 44 (4) (1999) 291–433.

[4] G. Herzer, Modern soft magnets: Amorphous and nanocrystalline materials, Acta Materialia 61 (3) (2013) 718–734.

[5] L. Rossi, O. Brüning, et al., High luminosity large hadron collider, in: European Strategy Preparatory Group-Open Symposium, Krakow, 2012.

[6] G. Ambrosio, Nb3Sn high field magnets for the high luminosity LHC upgrade project, IEEE Transactions on Applied Superconductivity 25 (3) (2015) 1–7.

[7] K. Dahlerup-Petersen, R. Denz, J. Gomez-Costa, D. Hagedorn, P. Proudlock, F. Rodrinuez-Mateos, R. Schmidt, F. Sonnemann, The protection system for the superconducting elements of the large hadron collider at cern, in: Particle Accelerator Conference, 1999. Proceedings of the 1999, Vol. 5, IEEE, 1999, pp. 3200–3202.

[8] R. Denz, E. De Matteis, A. Siemko, J. Steckert, Next generation of quench detection systems for the high luminosity upgrade of the lhc, IEEE Transactions on Applied Superconductivity 27 (4) (2017) 1–4.

[9] E. De Matteis, D. Calcoen, R. Denz, A. Siemko, J. Steckert, M. Storkensen, New method for magnet protection systems based on a direct current derivative sensor, IEEE Transactions on Applied Superconductivity 28 (3) (2018) 1–5.

[10] V. Vacuumschmelze, Nanocrystalline cut cores made of vitroperm 500 for transformers (2016). URL https://www.vacuumschmelze.com/fileadmin/Medienbiliothek_2010/Unternehmen/Qualitaet/SD_Sicherheitsdatenblaetter/HT/IB43E.pdf

[11] I.-I. E. Commission, et al., Magnetic materials-part 4: Methods of measurement of dc magnetic properties of magnetically soft materials (2000).

[12] G. Taurelli, Development of a software module for the Simple Analogue Function Generator used by the CERN Complex Accelerator, Master's thesis, Universita di Pisa, presented on 26 Oct 2005 (2005). URL http://cds.cern.ch/record/1258397

[13] J. D. Ramboz, Machinable rogowski coil, design, and calibration, IEEE Transactions on Instrumentation and measurement 45 (2) (1996) 511–515.

[14] D. G. Pellinen, M. S. Di Capua, S. E. Sampayan, H. Gerbracht, M. Wang, Rogowski coil for measuring fast, high-level pulsed currents, Review of Scientific instruments 51 (11) (1980) 1535–1540.